Available online at www.sciencedirect.com

ScienceDirect

Biomedical Journal

journal homepage: www.elsevier.com/locate/bj

Original Article

Gastrodia elata and parishin ameliorate aging induced 'leaky gut' in mice: Correlation with gut microbiota

Cai-xia Gong [a,b,1], Cheng Ma [c,1], Dejene Disasa Irge [d], Shu-min Li [a,b], Si-min Chen [a,b], Shi-xian Zhou [a,b], Xin-xiu Zhao [a,b], Han-yu Li [a,b], Jin-you Li [a,b], Yun-mei Yang [a,b,***], Lan Xiang [d,**], Qin Zhang [a,b,*]

[a] Department of Geriatrics, The First Affiliated Hospital, School of Medicine, Zhejiang University, Hangzhou, Zhejiang Province, China

[b] Zhejiang Provincial Key Laboratory for Diagnosis and Treatment of Aging and Physic-chemical Injury Diseases, The First Affiliated Hospital, School of Medicine, Zhejiang University, Hangzhou, Zhejiang province, China

[c] Protein Facility, Zhejiang University School of Medicine, Zhejiang University, Hangzhou, Zhejiang province, China

[d] College of Pharmaceutical Sciences, Zhejiang University, Hangzhou, Zhejiang province, China

ARTICLE INFO

Article history:
Received 23 June 2021
Accepted 2 July 2022
Available online 7 July 2022

Keywords:
Aging
Gastrodia elata
Parishin
Fecal microbiota
Intestinal barrier function
Inflammation

ABSTRACT

Background: The aging-induced decrease in intestinal barrier function contributes to many age-related diseases. Studies on preventive measures for "leaky gut" may help improve the quality of life of geriatric patients. The potent anti-aging effect of *Gastrodia elata* and parishin, which is one of its active ingredients, has been reported previously. However, their effects on the gut remain elusive, and the effect of parishin on mammals has not been studied.

Methods: We used quantitative RT-PCR, western blotting, immunohistochemical analysis, and 16S rRNA sequencing to investigate the effect of *G. elata* and parishin on the intestinal barrier function of D-Gal-induced aging mice.

Results: *G. elata* and parishin prevented the decrease in tight junction protein (TJP) expression and morphological changes, modulated the composition of fecal microbiota to a healthier state, and reversed the translocation of microbial toxins and systemic inflammation. The correlation analyses showed that TJP expression and systemic inflammation were significantly positively or negatively correlated with the composition of fecal microbiota after *G. elata* and parishin administration. Additionally, TJP expression was also correlated with systemic inflammation. Moreover, *G. elata* and parishin administration reversed the decreased or increased expression of aging-related biomarkers, such as FOXO3a, SIRT1, CASPASE3 and P21, in the gut.

* Corresponding author. Department of Geriatrics, The First Affiliated Hospital, School of Medicine, Zhejiang University, Hangzhou, Zhejiang, China.
** Corresponding author.
*** Corresponding author. Department of Geriatrics, The First Affiliated Hospital, School of Medicine, Zhejiang University, Hangzhou, Zhejiang, China.
E-mail addresses: 1194070@zju.edu.cn (Y.-m. Yang), lxiang@zju.edu.cn (L. Xiang), zhangqin1978@zju.edu.cn (Q. Zhang).
Peer review under responsibility of Chang Gung University.
[1] These authors have contributed equally to this work and share first authorship.
https://doi.org/10.1016/j.bj.2022.07.001

Conclusions: These results suggested that *G. elata* and parishin could prevent gut aging and ameliorate the "leaky gut" of aged mice and that the underlying mechanism is related to the mutual correlations among barrier function, fecal microbiota composition, and inflammation.

At a glance commentary

Scientific background on the subject

As the first barrier to prevent the invasion of pathogens, the "gut aging" contributes to many age-related diseases. Recently, accumulating evidences has indicated that *Gastrodia elata* and parishin had anti-aging activities. But their effects on "gut aging" have not been examined.

What this study adds to the field

This study demonstrated the anti-aging effect of *Gastrodia elata* and parishin on gut, and the underlying mechanism was correlated with the modulation of the composition of fecal microbiota. Our study will be helpful for the anti-aging medicine development and new therapeutic effect researching of *Gastrodia elata*.

Introduction

Aging is a highly complex process affecting many physiological, genomic, metabolic, and immunological functions. It is only recently that progress in cellular and molecular research has enabled a clearer understanding of the various mechanisms that underlie the complex processes of age-associated disturbances, including inflammation and metabolic dysfunctions [1,2]. With the aggravation of aging problems, research on anti-aging strategies has become extremely urgent for aging and age-related diseases. In addition to brain aging (which is the focus of most anti-aging investigations), the gut (which is regarded as the beginning of all diseases [3]) also deserves investigation for the prevention and treatment of gut aging.

The gut is the largest interface between the human body and the external environment and is the first barrier to prevent the invasion of pathogens. It comprises many microorganisms that form a symbiosis with the host during the long-term evolution process. Under normal circumstances, these microorganisms do not damage the health of the body, mainly owing to the complete intestinal mucus barrier function. However, intestinal permeability, indicating mucosal barrier integrity, increases with age ("leaky gut") and contributes to the occurrence of age-related diseases [4,5]. Studies on the mechanism and protective measures of intestinal barrier dysfunction may help improve the quality of life of geriatric patients.

Aging is considered a chronic inflammatory state [6]. With the increase in age, the immune system undergoes complex changes [7] that induce the production of pro-inflammatory cytokines, such as interleukin- 6 (IL-6), interleukin-1β (IL-1β), and tumor necrosis factor-α (TNF-α) [8]. An increase in pro-inflammatory factor levels directly affects intestinal permeability [9–12], which causes the translocation of toxins and aggravates the inflammatory state of the host [3].

Additionally, aging induces gut microbiota changes [2,13–17]. For instance, the abundance of the *Firmicutes* phylum, the metabolic product of which is butyrate (which has a preventive effect on the intestine [18]), significantly decreases; however, the abundance of the *Bacteroidetes* phylum, a lipopolysaccharide (LPS)-secreting gram-negative bacteria, significantly increases during aging [13–15]. Moreover, microbiota dysbiosis could affect host aging, including intestinal barrier immunity and systemic inflammation [16,17,19–21].

Gastrodia elata is a commonly used traditional Chinese medicine for its sedative, anti-anxiety, and anti-vertigo effects and as a treatment for central nervous system diseases. Accumulating evidence has indicated that *G. elata* had health-promoting features on aging-related diseases, including memory improvement and neuroprotective activities [22–24]. However, the effects of *G. elata* on gut aging remain elusive. Parishin, one of its active ingredients, can prolong the lifespan of yeast [25]; however, its effect on mammals has not been examined. In this study, we used quantitative reverse transcription (RT)-PCR, western blotting, immunohistochemical analysis, and 16S rRNA sequencing to investigate the effect of *G. elata* on the gut using a D-Gal-induced aging mouse model. As parishin may be more suitable for drug development as a single substance, we also tested the effects of parishin. Our study will be helpful for the anti-aging medicine development and new therapeutic effect researching of *G. elata*.

Materials and methods

G. elata *and parishin preparation*

The *G. elata* used in this study was a powder of gastrodia capsules (Guizhou Yikang Pharmaceutical Co., Ltd., Guizhou, China), purchased from the First Affiliated Hospital of Medicine School of Zhejiang University, Hangzhou, China. Parishin was isolated from *G. elata*. Dried and crushed rhizomes of *G. elata* were extracted in 80% aqueous methanol at room temperature under constant shaking for 24 h. The extract obtained was filtered, and the solvent was removed using a rotary evaporator at 37 °C in a water bath. The crude extract (160 g) was suspended in water and partitioned with ethyl acetate. The water layer (112 g) was subjected to an ODS open column using a methanol:water (30:70, 40:60, 50:50, 60:40, 70:30, 90:10, and 100:0) solvent system. All fractions were analyzed by TLC, and fractions obtained from 40:60 (methanol:water) were further separated by silica open column using a dichloromethane:methanol (95:05, 90:10, 80:20, 75:25,

70:30, 60:40, 50:50, and 0:100) solvent combination. After TLC analysis, fractions obtained from 70:30 and 60:40 (600 mg) were mixed and subjected to HPLC (SP ODS-A (20 × 250), mobile phase, 35% aq. methanol, flow rate 8 mL/min) to yield a pure active compound (400 mg, $t_R = 26$ min). The structure of the compound was identified as parishin by comparing ^{1}H NMR and ^{13}C NMR data with those reported in Ref. [25] [Figs. S1A and B]. ^{1}H NMR (500 MHz, CD_3OD): δ = 2.77 (2H, *d*, *J* = 15.22 Hz), 2.94 (2H, *d*, *J* = 15.26 Hz), 3.37–3.48 (12H, m), 3.69 (3H, *dd*, *J* = 4.95, 12.03), 3.38 (3H, *dd*, *J* = 1.5, 12.0 Hz), 4.90–5.02 (9H, m), 7.04 (2H, *d*, *J* = 8.7 Hz), 7.07 (4H, *d*, *J* = 7.9 Hz), 7.16 (2H, *d*, *J* = 8.6 Hz), 7.24 (4H, *dd*, *J* = 2.0, 8.6 Hz), and ^{13}C NMR (500 MHz, CD_3OD): δ = 44.7 (2C), 62.5 (3C), 67.3 (2C), 68.2 (1C), 71.3 (3C), 74.7 (1C), 74.9 (1C), 77.9 (3C), 78.1 (3C), 102.2 (3C), 117.8 (6C), 130.7 (3C), 131.1 (6C), 159.1 (3C), 170.9 (2C), and 174.3 (1C).

Animal experimental design and tissue collection

Fifty-four 6-week-old male C57/BL6 mice were purchased from Shanghai Sake Experimental Animal Co., Ltd. The mice were housed in the experimental animal center of the First Affiliated Hospital of Medicine School of Zhejiang University, at a temperature of 22 ± 1 °C and humidity of 50% ± 5%, and maintained under a 12 h light/dark cycle.

After two week's acclimation period, mice were randomly divided into six groups (n ≥ 8 per group): control group (0.9% saline ip + 0.9% saline ig, n = 8), D-Gal group (420 mg/kg/d D-Gal ip + 0.9% saline ig, n = 8), *G. elata* group (420 mg/kg/d D-Gal ip + 0.8 g/kg/d *G. elata* ig, n = 10), parishin high-dose group (420 mg/kg/d D-Gal ip + 20 mg/kg/d parishin ig, n = 9), parishin mid-dose group (420 mg/kg/d D-Gal ip + 10 mg/kg/d parishin ig, n = 10), and parishin low-dose group (420 mg/kg/day D-Gal ip + 1 mg/kg/d parishin ig, n = 9). After 8 weeks of treatment, the pellets were collected for fecal microorganism investigation. At the end of the experiment, the mice were deprived of food for 4 h to empty the intestines.

Three mice in each group were anesthetized with 4% chloral hydrate and perfused with PBS and 4% paraformaldehyde for immunohistochemistry. The small intestine (jejunum/ileum) was removed and transferred to 4% paraformaldehyde for 24 h; then, it was dehydrated using a gradient of ethanol and embedded in paraffin for future analysis and long-term preservation. The remaining mice in each group were anesthetized with 4% chloral hydrate, and whole blood was collected from the mouse orbit. The small intestine was removed and collected. All tissues were quickly frozen in liquid nitrogen and stored at −80 °C for long-term preservation.

Intestinal morphology and histology investigation

Intestinal paraffin-embedded tissues were cut into 3-μm thick slices. Slices were stained with hematoxylin & eosin (H&E) or Alcian blue (AB) and observed under a 3D HISTECH PL250 instrument (3D HISTECH, Magyarország). The intestinal villus height, width, and area were measured using 3D HISTECH slide converter 2.1 (3D HISTECH, Magyarország) and ImageJ (NIH, https://imagej.nih.gov/ij/) software. Photographs were obtained using 3D HISTECH's slide converter software.

Quantitative RT-PCR analysis

Total RNA of the frozen intestinal tissue was extracted using Trizol reagent (CW0580s, CWBIO, China) according to the manufacturer's instructions. cDNA synthesis was performed using the PrimeScript RT Reagent Kit (RR037A, Takara, Japan). Next, 2 μg of total RNA from each sample was used for cDNA synthesis. Quantitative RT-PCR was performed using TB Green Premix EX Taq (RR420A, Takara, Japan) on a Roche 480II high-throughput fluorescent quantitative PCR system (Roche, Germany). Actin was used as a reference gene. Relative mRNA expression was calculated using the 2−ΔΔCt method. Primers were synthesized by Shanghai Sangon Biotech Co., Ltd. (Shanghai, China). The primer sequences used for quantitative PCR were as follows: Tjp2-F, 5'-CGGATTCCAGACAAGGTGTT-3'; Tjp2-R, 5'-ATTCACGTTGATTGTGGCTG-3'; β-actin-F: 5'-AACAGTCCGCCTAGAAGCAC-3', β-actin-R: 5'-CGTTGACATCCGTAAAGACC-3'.

Western blot analysis

Collected tissues were ground in a strong radioimmunoprecipitation assay (RIPA) (CW2333s, CWBIO, Taizhou, China) lysis buffer with 1% protease inhibitor cocktail (CW2200s, CWBIO, Taizhou, China). The protein concentration was determined using a BCA Protein Assay Kit (CW0014s, CWBIO, Taizhou, China). Then, 10 μg protein for TJP2, CASPASE3 and P21, and 20 μg protein for FOXO3A and SIRT1 of each sample were subjected to electrophoresis on 4%–20% gradient ExpressPlus PAGE Gels (M42015C, GenScript, Nanjing, China) and transferred to pure nitrocellulose transfer membranes (1215458, GVS, Sanford, USA). After blocking with 3% bovine serum albumin (AR2440, BBI Life Sciences, Shanghai, China) for 2 h at room temperature, the membranes were incubated with primary antibodies that were targeted against TJP2 (ab191133, 1:1000, Abcam, Cambridge, England), β-ACTIN (CW0096M, 1:5000, CWBIO, Taizhou, China), CLEAVED CASPASE3 (9664, 1:1000, CST, Boston, USA), P21 (sc-6246, 1:2000, SANTA CRUZ, Santa Cruz, USA), FOXO3A (12829, 1:500, CST, Boston, USA), SIRT1 (ac110304, 1:1000, Abcam, Cambridge, England) overnight at 4 °C. After washing three times with TBST, these membranes were incubated with HRP-conjugated secondary antibodies (goat anti-rabbit IgG, CW0103s, 1:5000, CWBIO, Taizhou, China; goat anti-mouse IgG, CW0102s, 1:5000, CWBIO, Taizhou, China) for 2 h at room temperature and visualized using chemiluminescence solution (WBKLS0100, Millipore, Massachusetts, USA) after washing. Semi-quantitative band intensity measurements were performed using ImageJ software (NIH, https://imagej.nih.gov/ij/).

16S rRNA sequencing of fecal microbiota and processing of sequencing data

To ensure adequate samples and stable sequencing results, 1 day before euthanasia, fecal samples from the whole day were collected, quickly frozen in liquid nitrogen, and stored at −80 °C before DNA extraction and analysis. DNA extraction, sequencing, and analysis were conducted by BGI Co., Ltd.

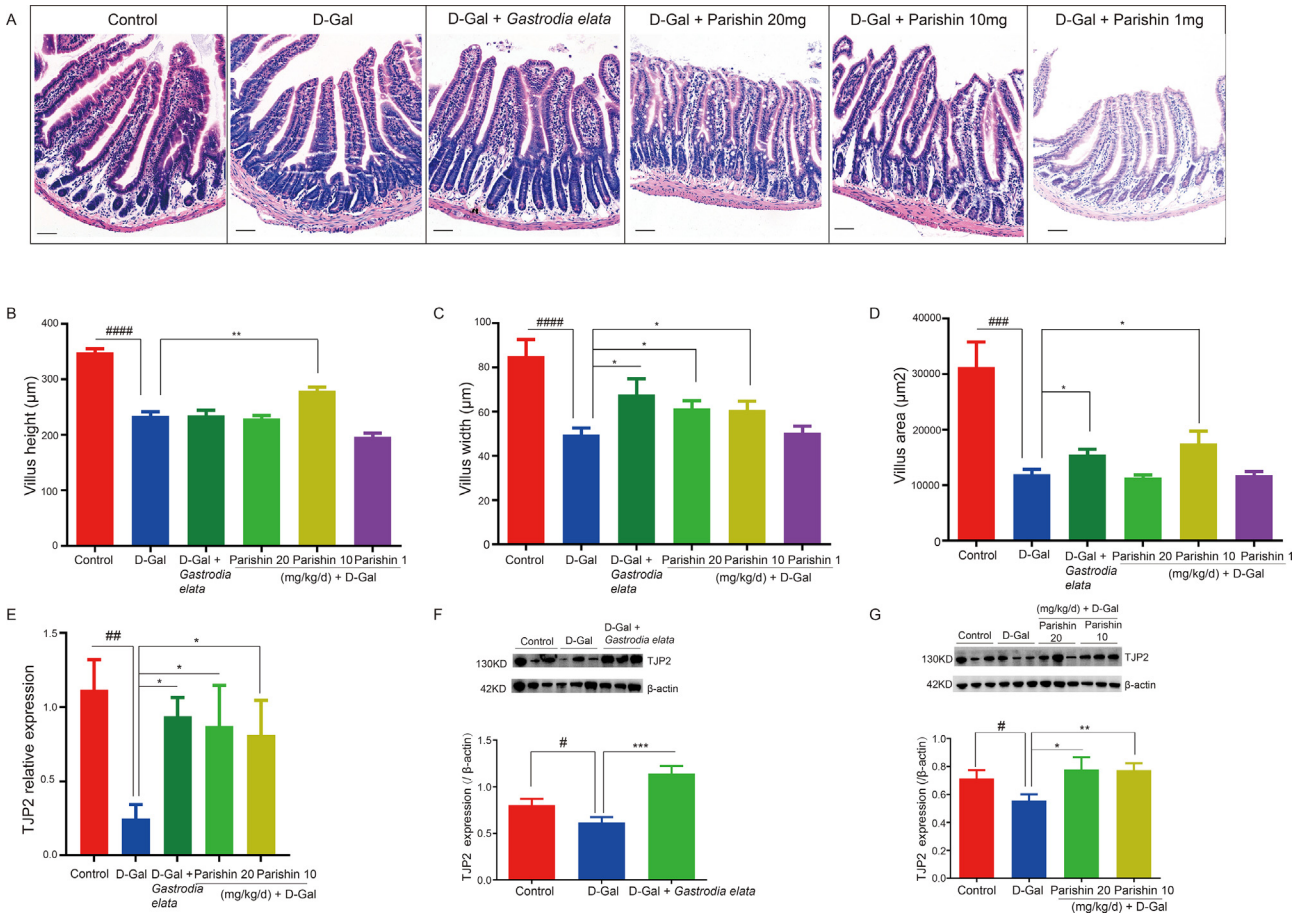

Fig. 1 Effect of *G. elata* and parishin on D-Gal induced morphological changes and intestinal tight junction protein (TJP) expression in the small intestine. (A) Representative pictures of morphological changes in the small intestine using HE staining. Scale bar, 50 μm. (B, C, and D) Quantification of villus height, width, and surface area in the intestine. Three mice in each group. ####, $p < 0.0001$, ###, $p < 0.001$, represent significant differences between the control group and D-Gal group. *, $p < 0.05$, **, $p < 0.01$, indicate significant differences between treatment groups and D-Gal group. The not labeled groups were not significantly different compared to the D-Gal group. (E) Effect of *G. elata* and parishin on the mRNA expression level of *tjp2* in the intestine analyzed by RT-PCR. n ≥ 4 for each group. ##, $p < 0.01$, represents significant differences between the control and D-Gal groups. *. $p < 0.05$, indicates significant differences between *G. elata* treatment group and D-Gal group. (F) Effect of *G. elata* on the protein expression level of TJP2 in the intestine analyzed by western blotting. n = 3 for each group. The histogram is the quantitative results. #, $p < 0.05$, represents significant differences between the control and D-Gal groups. ***, $p < 0.001$, indicates significant differences between *G. elata* treatment group and D-Gal group. (G) Effect of parishin on the protein expression level of TJP2 in the intestine analyzed by western blotting. n = 3 for each group. The histogram is the quantitative results. #, $p < 0.05$, represents significant differences between the control group and D-Gal group. *, $p < 0.05$, **, $p < 0.01$, indicate significant differences between parishin treatment group and D-Gal group.

(Shenzhen, China). The analysis process is presented in Supplementary Information.

LPS and pro-inflammatory cytokines investigation

The whole blood of animals was collected from mouse orbits, rested for 2 h at room temperature, and centrifuged at 3000 rpm for 15 min; supernatants were sub-packed and stored at −80 °C for future analysis. Serum, gut and fecal LPS (SU-BN20839), serum pro-inflammatory cytokines, IL-6 (SU-BN20188), IL-1β (SU-BN20174), and TNF-α (SU-BN20852), were tested using mouse ELISA kits (Ruixin Biotech, Quanzhou, China) according to the manufacturer's instructions.

Statistical analysis

Data are presented as the mean ± SEM and were analyzed using GraphPad Prism version 6 (GraphPad Software Inc, USA). The quantitative results of HE staining alcian blue staining (AB staining), RT-PCR, and Western blot were analyzed using an unpaired t test. Other results were analyzed using the Mann–Whitney test. The correlation coefficient was analyzed

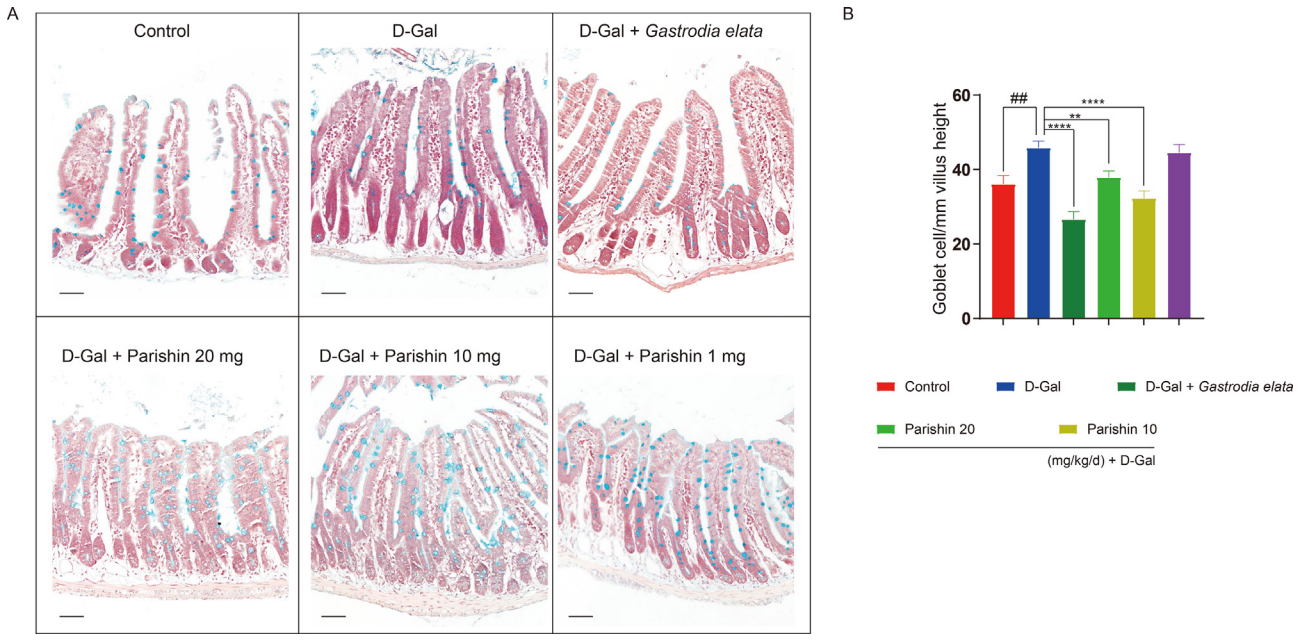

Fig. 2 Effect of *G. elata* and parishin on intestinal mucus layer constituted chemical barrier function. (A) Representative pictures of AB staining, Scale bar, 50 μm. (B) Quantification of goblet cells in the intestine. Three mice in each group. ##, $p < 0.01$, represents significant differences between the control group and D-Gal group. ****, $p < 0.0001$, **, $p < 0.05$, indicate significant differences between treatment groups and D-Gal group. The not labeled groups were not significantly different compared to the D-Gal group.

using Spearman correlation analysis. A p value of less than 0.05 was considered statistically significant.

Results

Recovery of morphology and barrier function of the intestine after administration of G. elata *and parishin*

D-Gal-induced aging models have symptoms similar to natural aging [26]. We tested the effect of *G. elata* and parishin on aging using a D-Gal-induced aging model. The intestinal epithelial cells and tight junctions between them mainly constitute the mechanical barrier of the gut; therefore, to test the effect of *G. elata* and parishin on the mechanical barrier, we investigated the morphological changes after administration [Fig. 1A]. The villus height, width, and area were measured using image analysis software. These indices were significantly lower in D-Gal-induced aging mice than in the control mice [Fig. 1B–D]. *G. elata* treatment increased the villus width and area [Fig. 1C and D]. Treatment with 20 mg/kg/d parishin increased the villus width [Fig. 1C], and the administration of 10 mg/kg/d parishin increased all three indices [Fig. 1B–D], whereas 1 mg/kg/d parishin treatment had no effect. These results suggested that *G. elata* and 10 and 20 mg/kg/d parishin treatment could rescue (at least in part) the villus morphological changes in D-Gal-induced aging mice. We then tested the expression levels of TJP. On the mRNA level, the expression levels of *tjp2* decreased in D-Gal-induced model mice compared with control mice [Fig. 1E]. *G. elata* and 10 and 20 mg/kg/d parishin treatment reversed this effect [Fig. 1E]. This observation was confirmed by western blotting. As expected, TJP2 expression on the protein level significantly decreased in D-Gal mice [Fig. 1F and G]. *G. elata* and 10 and 20 mg/kg/d parishin significantly reversed this effect [Fig. 1F and G].

The mucus layer secreted by intestinal epithelial cells can isolate many foreign substances that contact the epithelial cells and mainly constitutes the chemical barrier of the intestine. Therefore, we investigated the mucus layer in the intestine using AB staining and found more mucus layer detachments in D-Gal mice than in control mice. Interestingly, *G. elata* and parishin administration rescued these effects [Fig. 2A]. In addition, the number of goblet cells, which are specific for mucus secretion, was significantly elevated in D-Gal mice [Fig. 2B], whereas *G. elata* and 10 and 20 mg/kg/d parishin significantly reversed this effect [Fig. 2B]. These results revealed that *G. elata* and parishin could rescue intestinal mucosal mechanical and chemical barrier function induced by D-Gal.

Effect of G. elata *and parishin on fecal microbiota composition*

Aging induces changes in fecal microorganisms. Mice pellets were collected 8 weeks after treatment, and total fecal microbiota profiles were analyzed by 16S rRNA amplicon sequencing to test the effect of *G. elata* and parishin on fecal microbiota composition. Sequences were grouped into clusters as operational taxonomic units (OTUs). Using principal component analysis (PCA) based on OTUs, we revealed a shift in the fecal microbiota composition between D-Gal and control mice. Among all administration groups, 10 mg/kg/d parishin reversed the fecal microbiota composition to a level closer to that of the control mice [Fig. 3A].

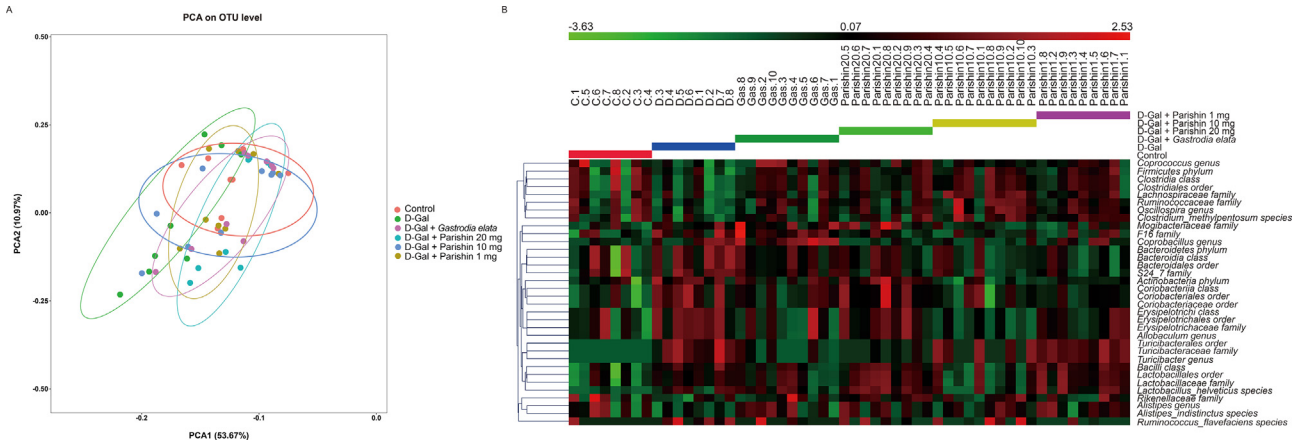

Fig. 3 Effect of *G. elata* and parishin on fecal microbiota composition changes induced by D-Gal. (A) Results of PCA based on OTUs after *G. elata* and parishin treatment. (B) Heatmap of relative abundances of fecal microbiota that was significantly different or had large change trends among control group, D-Gal group, *G. elata* and parishin treatment groups at phylum, class, order, family genus, and species levels. n = 8, 8, 10, 9, 10, and 9 for control, D-Gal, D-Gal + *G. elata*, D-Gal + 20 mg/kg/d parishin, D-Gal + 10 mg/kg/d parishin, and D-Gal + 1 mg/kg/d parishin, respectively.

To further study the effect of *G. elata* and parishin on gut microbial composition, we analyzed phylum, class, order, family, genus, and species levels, respectively. The heatmap of the mainly affected microbiota in the D-Gal and *G. elata* and parishin administration groups is shown in Fig. 3B. The relative abundance of these gut microbiota types and their taxon relationships are shown in Fig. S2.

At the phylum level, the relative abundance of *Actinobacteria* was significantly higher in the D-Gal group than in the control group [Fig. S2A1]. After 8 weeks of administration of 1 and 10 mg/kg/d parishin, its abundance was significantly decreased to normal levels [Fig. S2A1]. However, 20 mg/kg/d parishin and *G. elata* treatment had no significant effect. For the two major components, *Firmicutes* and *Bacteroidetes*, there was a downward and upward tendency, respectively, in the D-Gal group compared with the control group [Fig. S2A2 and A3], similar to previous results [13–15]. Mice treated with 10 and 20 mg/kg/d parishin significantly increased the abundance of *Firmicutes* [Fig. S2A2], and the administration of 1 and 10 mg/kg/d parishin significantly decreased the abundance of *Bacteroidetes* [Fig. S2A3].

At the class level, the relative abundance of *Coriobacteriia*, affiliated with the *Actinobacteria* phylum, and that of *Bacilli* and *Erysipelotrichi*, affiliated with the *Firmicutes* phylum, were significantly higher in the D-Gal group than in the control group [Fig. S2B1–B3]. Treatment with 1 mg/kg/d parishin significantly reversed the increase in *Coriobacteriia* abundance [Fig. S2B1]. *G. elata* and 1 and 10 mg/kg/day parishin administration significantly reversed the increase in *Erysipelotrichi* abundance [Fig. S2B3]. For the two major components, *Clostridia*, which was affiliated with the *Firmicutes* phylum, and *Bacteroidia*, which was affiliated with the *Bacteroidetes* phylum, the changes in the D-Gal group were similar to their parent phyla [Fig. S2B4 and B5]. *G. elata* and parishin administration reversed the abundance change trends in the D-Gal group; especially for *Clostridia*, all treatments significantly decreased the increase in the D-Gal group [Fig. S2B4]. The abundance of *Bacteroidia* significantly decreased after 1 and 10 mg/kg/d parishin treatment [Fig. S2B5].

At the order level, the relative abundances of *Coriobacteriales*, affiliated with the *Coriobacteriia* class, *Lactobacillales*, affiliated with the *Bacilli* class, and *Turicibacterales* and *Erysipelotrichales*, affiliated with the *Erysipelotrichi* class, were significantly higher in the D-Gal group than in the control group [Fig. S2C1–C3]. The effects of *G. elata* and parishin treatment on the abundance of *Coriobacteriales*, *Lactobacillales*, and *Erysipelotrichales* were similar to their parent classes [Fig. S2C1–C3]. In addition, *G. elata* and 20 mg/kg/d parishin treatment significantly decreased the abundance of *Turicibacterales* [Fig. S2C2]. The changes in the abundance of the two major components, *Clostridiales*, affiliated with the *Clostridia* class, and *Bacteroidales*, affiliated with the *Bacteroidia* class, among all groups were similar to their parent classes [Fig. S2C4 and C5].

Changes in the relative abundance of Coriobacteriaceae, Lactobacillaceae, *Turicibacteraceae*, and Erysipelotrichaceae at the family level, affiliated with the order *Coriobacteriales*, *Lactobacillales*, *Turicibacterales*, and *Erysipelotrichales*, respectively, were similar to their parent orders among all groups [Fig. S2D1–D3]. The abundance of Ruminococcaceae and Lachnospiraceae, which were affiliated with the order *Clostridiales*, was lower in the D-Gal group than in the control group [Fig. S2D3 and D4]. The administration of 1 and 10 mg/kg/d parishin significantly increased the abundance of Ruminococcaceae [Fig. S2D3], and 10 mg/kg/d parishin treatment significantly increased the abundance of Lachnospiraceae [Fig. S2D4]. *S24-7* and *F16*, which were affiliated with the order *Bacteroidales*, showed a rising trend in the D-Gal group compared with the control group [Fig. S2D5 and D6]. All treatment groups reversed the changes in the *S24-7* family in trend, and all three doses of parishin caused a significant reversal [Fig. S2D5]. Mice treated with 10 mg/kg/d parishin had a significantly decreased abundance of *F16* [Fig. S2D6]. The relative abundance of *Mogibacteriaceae*, which may be

affiliated with other orders and classes of the *Bacteroidetes* phylum, was significantly higher in the D-Gal group than in the control group [Fig. S2D6]. This effect was significantly reversed by treatment with 10 mg/kg/d parishin [Fig. S2D6].

At the genus level, the relative abundances of *Turicibacter*, affiliated with the *Turicibacteraceae* family, and *Coprobacillus* and *Allobaculum*, affiliated with the Erysipelotrichaceae family, were significantly higher in the D-Gal group than in the control group [Fig. S2E1 and E2]. The abundance of *Oscillospira*, affiliated with the Ruminococcaceae family, was significantly decreased in the D-Gal group [Fig. S2E2]. Changes in the genera *Turicibacter* and *Allobaculum* after *G. elata* and parishin treatment were similar to those of their parent families [Fig. S2E1 and E2]. All three doses of parishin significantly reversed the abundance of *Oscillospira* [Fig. S2E2].

At the species level, the relative abundances of *Lactobacillus_helveticus*, affiliated with other genera of the Lactobacillaceae family, and *Ruminococcus_flavefaciens*, affiliated with other genera of Ruminococcaceae family, were significantly increased in the D-Gal group [Fig. S2F1 and F2]. The

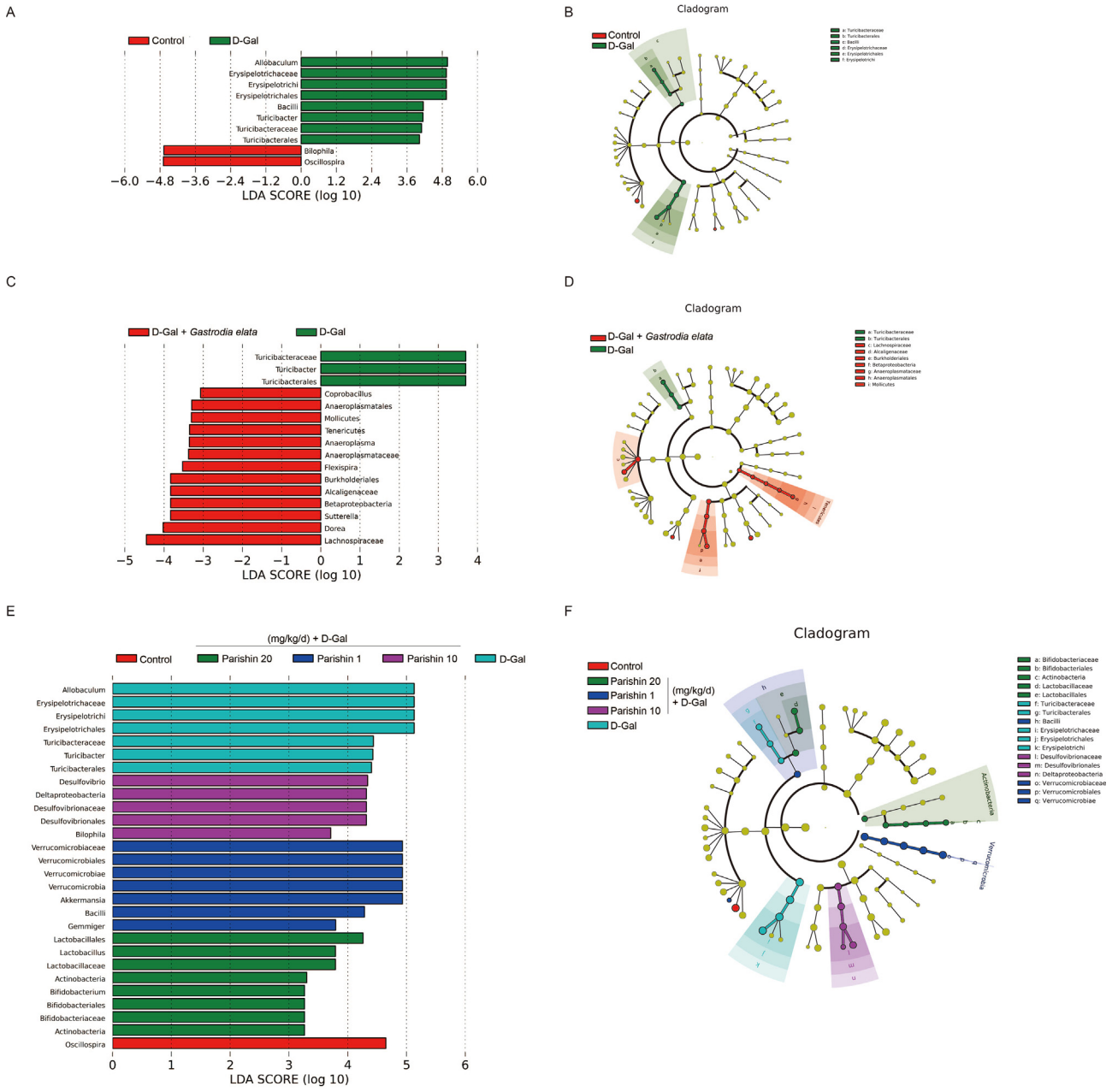

Fig. 4 LEfSe analysis results of fecal microbiota after administration of *G. elata* and parishin. (A and B) LEfSe analysis results of the fecal microbiota of the control and D-Gal groups. LDA score is shown in A. Cladogram is shown in B. (C and D) LEfSe analysis results of the fecal microbiota among the control group, D-Gal group, and *G. elata* administration group. LDA score is shown in C. Cladogram is shown in D. (E and F) LEfSe analysis results of the fecal microbiota among the control group, D-Gal group, and parishin treatment groups. LDA score is shown in E. Cladogram is shown in F. n = 8, 8, 10, 9, 10, and 9 for control, D-Gal, D-Gal + *G. elata*, D-Gal + 20 mg/kg/d parishin, D-Gal + 10 mg/kg/d parishin, and D-Gal + 1 mg/kg/d parishin, respectively.

administration of 1 mg/kg/d parishin significantly decreased the abundance of *Ruminococcus_flavefaciens* [Fig. S2F2]. The relative abundance of *Clostridium_methylpentosum*, affiliated with other families of the order *Clostridiales*, showed a decreasing trend [Fig. S2F3]. Treatment with 1 and 10 mg/kg/d parishin significantly increased its abundance [Fig. S2F3].

Linear discriminant analysis (LDA) effect size (LEfSe) analysis of the fecal microbiota after G. elata *and parishin treatment*

The LDA score and LEfSe analysis are shown in Fig. 4. Compared with the control group, *Allobaculum*, Erysipelotrichaceae, *Erysipelotrichi*, *Erysipelotrichales*, *Bacilli*, *Turicibacter*, *Turicibacteraceae*, and *Turicibacterales* were the main microorganisms in the D-Gal group. *Bilophila* and *Oscillospira* were the main microorganisms in the control group [Fig. 4A and B]. After *G. elata* administration, the abundances of *Turicibacteraceae*, *Turicibacter*, and *Turicibacterales* were significantly decreased [Fig. S1C2, D2, and E1]; these three were still the main microorganisms in the D-Gal group [Fig. 4C and D]. In addition, *Coprobacillus*, *Anaeroplasmatales*, *Mollicutes*, *Tenericutes*, *Anaeroplasma*, *Anaeroplasmataceae*, *Flexispira*, *Burkholderiales*, Alcaligenaceae, *Betaproteobacteria*, *Sutterella*, *Dorea*, and Lachnospiraceae were the main microorganisms in the *G. elata* administration group [Fig. 4C and D]. After parishin administration, *Allobaculum*, Erysipelotrichaceae, *Erysipelotrichi*, *Erysipelotrichales*, *Turicibacter*, *Turicibacteraceae*, and *Turicibacterales* remained the main microorganisms in the D-Gal group [Fig. 4E and F] as the abundances of these microorganisms in the control group and parishin administration groups were all lower than that in the D-Gal group [Fig. S2B3, C2, C3, D2, D3, E1, and E2]. Although parishin administration significantly increased the abundance of *Oscillospira*, *Oscillospira* was still the main microorganism in the control group [Fig. 4E and F]. In addition, *Lactobacillales*, *Lactobacillus*, Lactobacillaceae, *Actinobacteria*, *Bifidobacterium*, *Bifidobacteriales*, Bifidobacteriaceae, and *Actinobacteria* were the main microorganisms in the 20 mg/kg/d parishin group. *Desulfovibrio*, *Deltaproteobacteria*, Desulfovibrionaceae, *Desulfovibrionales*, and *Bilophila* were the main microorganisms in the 10 mg/kg/d parishin group. *Verrucomicrobiaceae*, *Verrucomicrobiales*, *Verrucomicrobiae*, *Verrucomicrobia*, *Akkermansia*, *Bacilli*, and *Gemmiger* were the main microorganisms in the 1 mg/kg/d parishin group. These results suggested that *G. elata* and parishin could regulate the gut microbiota changes caused by D-Gal.

PICRUST function analysis of the fecal microbiota after G. elata *and parishin treatment*

PICRUST predicted the relative abundance of fecal microbiota at three levels of the KEGG pathway. The results are shown in Fig. S3. At level 2, the abundances of the fecal microbiota in cancer and nucleotide metabolism pathways were significantly higher in the D-Gal group than in the control group [Fig. S3A]. Treatment with 10 and 20 mg/kg/d parishin significantly reversed the abundance of microorganisms in the cancer pathway [Fig. S3A]. *G. elata* and three doses of parishin significantly reversed the abundance of microorganisms in nucleotide metabolism pathways [Fig. S3A]. Furthermore, at level 3, the abundances of the fecal microbiota in G protein-coupled receptors, apoptosis, stilbenoid, diarylheptanoid and gingerol biosynthesis, renal cell carcinoma, pathways in cancer, polycyclic aromatic hydrocarbon degradation, and aminoacyl-tRNA biosynthesis KEGG pathways were significantly higher in the D-Gal group than in the control group [Fig. S3B]. The abundances of the microflora in steroid hormone biosynthesis, C5-Branched dibasic acid metabolism, valine, leucine and isoleucine biosynthesis, transcription machinery, and starch and sucrose metabolism pathways were significantly decreased in the D-Gal group [Fig. S3B]. *G. elata* administration significantly reversed the abundance of the microflora in G protein-coupled receptors, stilbenoid, diarylheptanoid, and gingerol biosynthesis, steroid hormone biosynthesis, pathways in cancer, polycyclic aromatic hydrocarbon degradation, C5-Branched dibasic acid metabolism, valine, leucine and isoleucine biosynthesis, transcription machinery, and aminoacyl-tRNA biosynthesis pathways [Fig. S3B]. Treatment with 20 mg/kg/d parishin significantly reversed the abundance of the microflora in G protein-coupled receptors, steroid hormone biosynthesis, pathways in cancer, polycyclic aromatic hydrocarbon degradation, C5-Branched dibasic acid metabolism, and aminoacyl-tRNA biosynthesis pathways [Fig. S3B]. Treatment with 10 mg/kg/d parishin significantly reversed the abundance of the microflora in stilbenoid, diarylheptanoid, and gingerol biosynthesis, pathways in cancer, polycyclic aromatic hydrocarbon degradation, C5-Branched dibasic acid metabolism, transcription machinery, and aminoacyl-tRNA biosynthesis pathways [Fig. S3B]. Treatment with 1 mg/kg/d parishin significantly reversed the abundance of the microflora in stilbenoid, diarylheptanoid, and gingerol biosynthesis, steroid hormone biosynthesis, and transcription machinery pathways [Fig. S3B].

Ameliorating effect of G. elata *and parishin on the inflammatory state of the mice in the blood induced by D-Gal*

Aging is a chronic inflammatory state. The abundances of inflammation-related and LPS-producing microbiota increased, while the intestinal barrier function decreased in D-Gal-induced aging mice in this study; therefore, we tested the effect of *G. elata* and parishin on the expression of LPS and inflammatory cytokines in the blood. As expected, LPS and pro-inflammatory cytokine IL-6, IL-1b, and TNF-α levels were significantly increased in the D-Gal group [Fig. 5A and B]. However, the levels of these biomarkers decreased after *G. elata* treatment [Fig. 5A and B]. Parishin treatment decreased the levels of these factors in a dose-dependent manner [Fig. 5A and B]. These results suggested that *G. elata* and 10 and 20 mg/kg/d parishin could significantly prevent the inflammatory state in the blood of D-Gal-induced aging mice. We also tested the LPS content in the gut and fecal, and found that the gut LPS of D-Gal mice increased in trend compared with control mice, and *G. elata* and parishin (10 and 20 mg/kg/d) could reverse it significantly [Fig. S4A]. Similar change trends were observed in fecal LPS, although without significant differences [Fig. S4C]. Comparing the ratio of LPS in serum with in gut and fecal [Figs. S4B and D], found that the ratio of serum and fecal

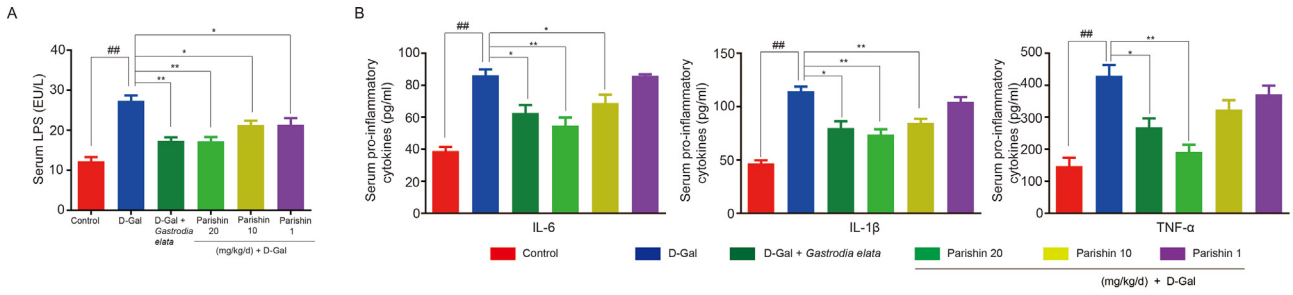

Fig. 5 Effect of *G. elata* and parishin on inflammatory state of the mice in blood. (A) Effect of *G. elata* and parishin on the increased expression level of serum LPS induced by D-Gal. (B) Effect of *G. elata* and parishin on the increased expression level of serum pro-inflammatory cytokines IL-6, IL-1β, and TNF-α induced by D-Gal. ##, $p < 0.01$, represents significant differences between the control and D-Gal groups. *. $p < 0.05$, **, $p < 0.01$, indicate significant differences between treatment groups and D-Gal group. The not labeled groups were not significantly different compared to the D-Gal group. n = 5, 5, 7, 6, 7, and 6 for control, D-Gal, D-Gal + *G. elata*, D-Gal + 20 mg/kg/d parishin, D-Gal + 10 mg/kg/d parishin, and D-Gal + 1 mg/kg/d parishin, respectively.

LPS significantly increased in D-Gal mice, and *G. elata* and parishin (20 mg/kg/d) could reverse it significantly [Fig. S4D], further confirmed the "leaky gut" in D-Gal mice, and the reverse effect of *G. elata* and parishin. Together, these results indicated that in aging mice, the level of LPS significantly increased, and the barrier function of the gut decreased, resulting in the translocation of LPS to peripheral blood.

Correlations among tjp2 expression, fecal microbiota composition, and inflammatory cytokines expression

Then, we performed a correlation analysis among *tjp2* expression, fecal microbiota composition, and inflammatory cytokines expression. The results showed that serum IL-6 expression was positively correlated with *Coriobacteriia* class [Fig. 6A], *Erysipelotrichi* class [Fig. 6B], *Turicibacterales* order [Fig. 6C], *Allobaculum* genus [Fig. 6B], and *Lactobacillus_helveticus* species [Fig. 6C] after *G. elata* administration. Moreover, serum IL-6 expression showed a non-significant but positive correlation with *Actinobacteria* phylum [Fig. 6A]. Serum IL-1β expression was positively correlated with *Coriobacteriia* class [Fig. 6D], *Turicibacterales* order [Fig. 6E] *Lactobacillus_helveticus* species [Fig. 6D], and *Ruminococcus_flavefaciens* species [Fig. 6 E] after *G. elata* administration. Furthermore, serum IL-1β expression showed a non-significant but positive correlation with *Bacilli* class [Fig. 6E], *Erysipelotrichi* class and *Allobaculum* genus [Fig. 6F], and a non-significant but negative correlation with *Clostridia* class [Fig. 6G]. Serum TNF-α expression was positively correlated with *Actinobacteria* phylum [Fig. 6H], *Coriobacteriia* class

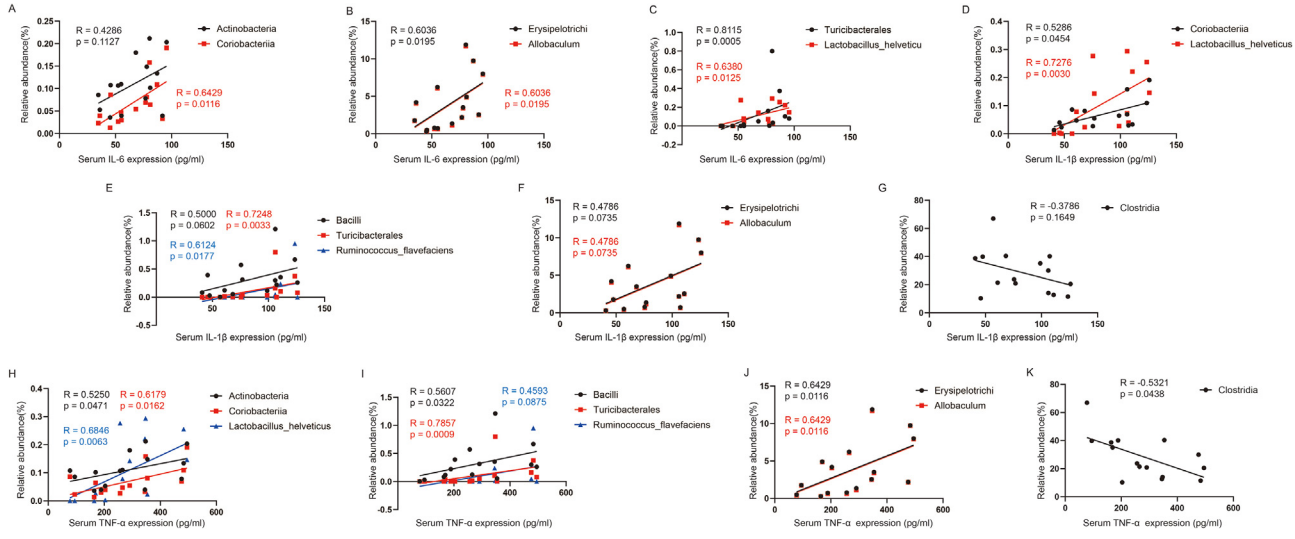

Fig. 6 Correlation coefficient between gut microbiota composition and inflammatory cytokines expression after *G. elata* administration. (A–C) Correlation coefficient of serum IL-6 expression and *Actinobacteria* (A), *Coriobacteriia* (A), *Erysipelotrichi* (B), *Allobaculum* (B), *Turicibacterales* (C), and *Lactobacillus_helveticus* (C). (D–G) Correlation coefficient of serum IL-1β expression and *Coriobacteriia* (D), *Lactobacillus_helveticus* (D), *Bacilli* (E), *Turicibacterales* (E), *Ruminococcus_flavefaciens* (E), *Erysipelotrichi* (F), *Allobaculum* (F), and *Clostridia* (G). (H–K) Correlation coefficient of serum TNF-α expression and *Actinobacteria* (H), *Coriobacteriia* (H), Lactobacillus_helveticus (H), *Bacilli* (I), *Turicibacterales* (I), *Ruminococcus_flavefaciens* (I), *Erysipelotrichi* (J), *Allobaculum* (J), and *Clostridia* (K).

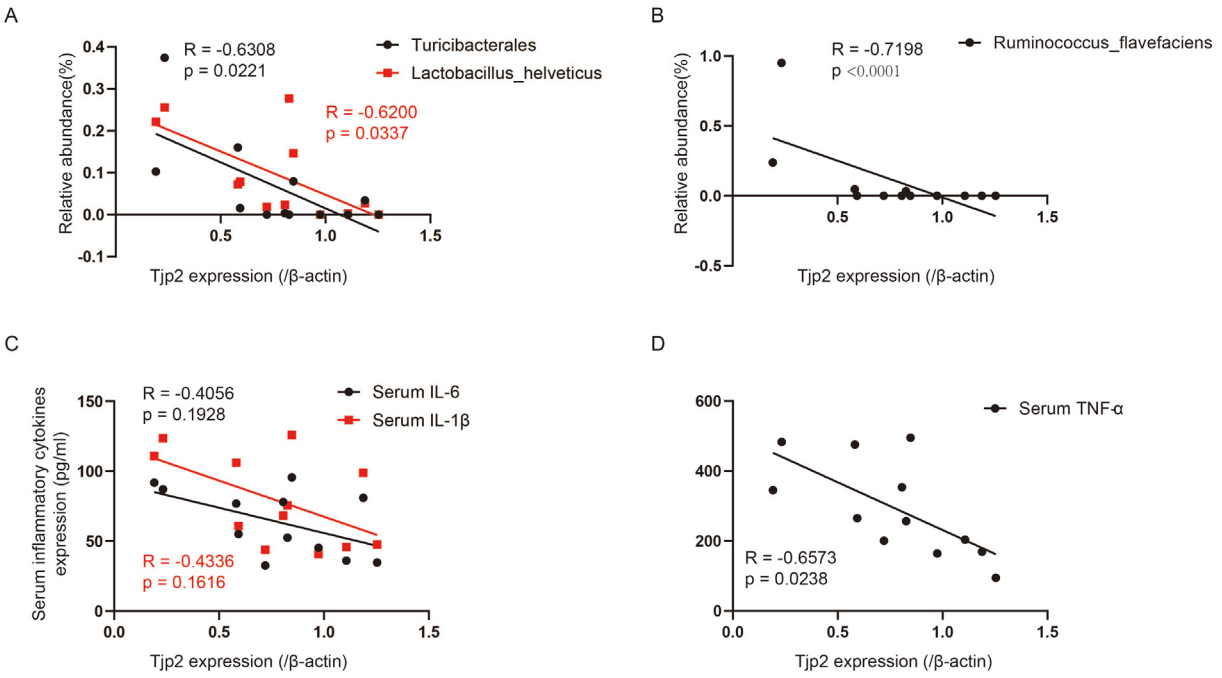

Fig. 7 Correlation coefficient between *tjp2* expression and fecal microbiota composition, *tjp2* expression and inflammatory cytokines expression after *G. elata* administration. (A and B) Correlation coefficient of *tjp2* expression and *Turicibacterales* (A), *Lactobacillus_helveticus* (A), and *Ruminococcus_flavefaciens* (B). (C and D) Correlation coefficient of *tjp2* expression and serum IL-6 expression (C), IL-1β expression (C), and TNF-α expression (D).

[Fig. 6H], *Bacilli* class [Fig. 6I], *Erysipelotrichi* class [Fig. 6J], *Turicibacterales* order [Fig. 6I], *Allobaculum* genus [Fig. 6J], and *Lactobacillus_helveticus* species [Fig. 6H]. Furthermore, serum TNF-α expression was negatively correlated with *Clostridia* class and non-significantly but positively correlated with *Ruminococcus_flavefaciens* species after *G. elata* administration [Fig. 6K and I]. The *tjp2* expression was also correlated with the fecal microbiota composition and the expression of the inflammatory cytokines after *G. elata* administration. In detail, *tjp2* expression was negatively correlated with *Turicibacterales* order, *Lactobacillus_helveticus* and *Ruminococcus_flavefaciens* species [Fig. 7A and B] and serum TNF-α expression [Fig. 7D]. Although not significant, *tjp2* expression was also negatively correlated with the serum IL-6 and IL-1β expression [Fig. 7C].

After parishin administration, correlations among fecal microbiota composition, *tjp2* expression, and inflammatory cytokines expression also existed. We used the most effective dose, 10 mg/kg/d parishin group, and the control and D-Gal groups to analyze these. The results showed that serum IL-6 expression was positively correlated with *Turicibacterales* order [Fig. 8C]. Although not significant, it was positively correlated with *Coriobacteriia* class [Fig. 8A], *Erysipelotrichi* and *Allobaculum* genus [Fig. 8B]. Serum IL-1β expression was negatively correlated with *Firmicutes* phylum and *Clostridia* class [Fig. 8D] and positively correlated with *Coriobacteriia*, *Bacilli* and *Erysipelotrichi* classes [Fig. 8E–G], *Turicibacterales* order [Fig. 8F], *Allobaculum* genus [Fig. 8G], and *Lactobacillus_helveticus* species [Fig. 8E]. Moreover, serum IL-1β expression was non-significantly but positively correlated with the *Ruminococcus_flavefaciens* species [Fig. 8F]. Serum TNF-α expression was non-significantly but positively correlated with the *Turicibacterales* order [Fig. 8H]. The *tjp2* expression was negatively correlated with *Coriobacteriia* and *Erysipelotrichi* classes [Fig. 9A and B], *Turicibacterales* order [Fig. 9C], *Mogibacteriaceae* family [Fig. 9A], *Allobaculum* genus [Fig. 9B], and *Lactobacillus_helveticus* species [Fig. 9C]. The *tjp2* expression was also negatively correlated with the serum IL-6 and IL-1β expression and non-significantly but negatively correlated with serum TNF-α expression [Fig. 9D and E]. These results suggested that the effects of *G. elata* and parishin on systemic inflammation, *tjp2* expression, and fecal microbiota composition were not independent. The effect on systemic inflammatory cytokines expression and *tjp2* expression was significantly correlated with the modulation of fecal microbiota composition; moreover, *tjp2* expression was also correlated with systemic inflammatory cytokines expression.

Effect of G. elata *and parishin on gut aging*

To further confirm the anti-aging effect of *G. elata* and parishin on gut aging, we tested the proteins expression of aging-related biomarkers in the gut, such as CLEAVED CASPASE3 and P21, which are related to apoptosis, and FOXO3A and SIRT1, which are linked to longevity [27,28]. The results showed that the protein levels of CLEAVED CASPASE3 and P21 were significantly higher in D-Gal mice than in control mice [Fig. 10A and B]. *G. elata* and 10 and 20 mg/kg/d parishin administration significantly decreased CASPASE3 expression

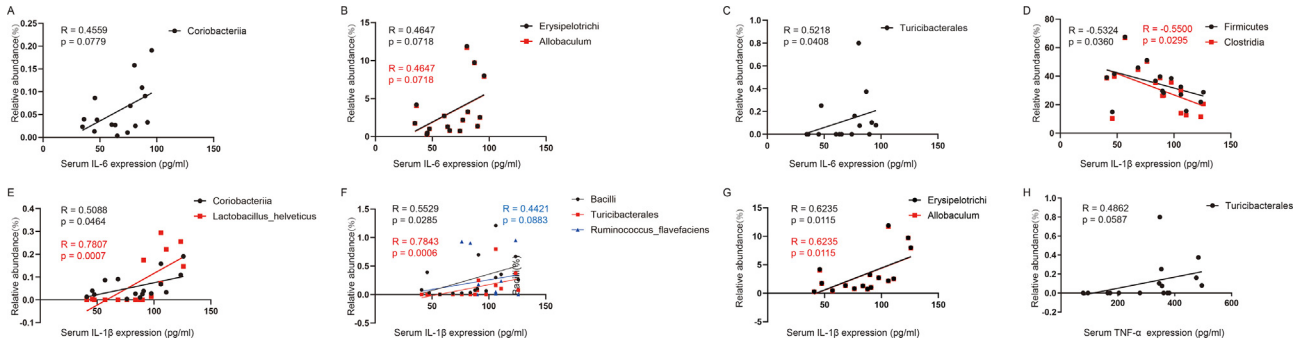

Fig. 8 Correlation coefficient between fecal microbiota composition and inflammatory cytokines expression after parishin administration. (A–C) Correlation coefficient of serum IL-6 expression and *Coriobacteriia* (A), *Erysipelotrichi* (B), *Allobaculum* (B), and *Turicibacterales* (C). (D–G) Correlation coefficient of serum IL-1β expression and *Firmicutes* (D), *Clostridia* (D), *Coriobacteriia* (E), *Lactobacillus_helveticus* (E), *Bacilli* (F), *Turicibacterales* (F), *Ruminococcus_flavefaciens* (F), *Erysipelotrichi* (G), and *Allobaculum* (G). (H) Correlation coefficient between serum TNF-α expression and *Turicibacterales*.

[Fig. 10A], whereas for P21, only 10 mg/kg/d parishin administration caused a significant reversed effect [Fig. 10B]. The proteins of FOXO3A and SIRT1 were significantly lower in D-Gal mice than in control mice [Fig. 10C]. *G. elata* administration elevated their expression, whereas 10 and 20 mg/kg/d parishin administration only increased the expression of SIRT1 [Fig. 10C]. These results suggested that *G. elata* and parishin could prevent gut aging via inhibition of CASPASE3, P21 and increase of SIRT1.

Discussion

In this study, we investigated the anti-aging effects of *G. elata* and parishin on the gut using a D-gal-induced aging mouse model, and demonstrated their protective effects on the gut from four aspects: *G. elata* and parishin prevented the D-Gal-induced decrease in intestinal barrier function and rescued the morphological changes in the villus; both *G. elata* and parishin treatments modulated the composition of fecal microbiota to a level similar to that of control mice; the administration of *G. elata* and parishin ameliorated the inflammatory state, as indicated by a decrease in biomarkers in blood; and *G. elata* and parishin reversed aging-related biomarker expression in the gut. Furthermore, the correlation analyses results showed that the protective effects on barrier function, fecal microbiota composition, and systemic inflammatory state were not independent and correlated significantly with each other. It is the first time that researchers have investigated the protective effect of *G. elata* on the gut, and the first investigation to demonstrate the potential anti-aging effect of parishin on mammals.

The results showed that the effects of parishin were not strictly dose-dependent. Generally, the effects of 10 and 20 mg/kg/d parishin were better than those of 1 mg/kg/d parishin [Figs. 1–3 and 5 and S2–S4], although 1 mg/kg/d parishin ameliorated the composition of some microbiota [Fig. S2]. In some instances, the effects of 20 mg/kg/d parishin were even inferior to those of 1 and 10 mg/kg/d parishin (Figs. 1 and S2]. Overall, 10 mg/kg/day parishin had the

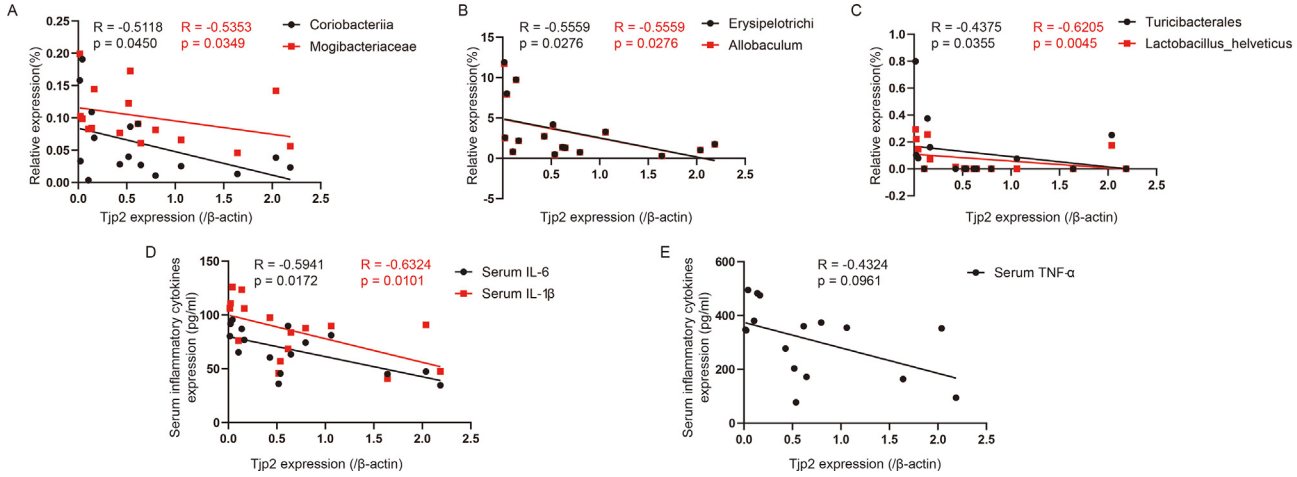

Fig. 9 Correlation coefficient between *tjp2* expression and fecal microbiota composition, *tjp2* expression and inflammatory cytokines expression after parishin administration. (A–C) Correlation coefficient of *tjp2* expression and *Coriobacteriia* (A), *Mogibacteriaceae* (A), *Erysipelotrichi* (B), *Allobaculum* (B), *Turicibacterales* (C), and *Lactobacillus_helveticus* (C). (D–E) Correlation coefficient of *tjp2* expression and serum IL-6 expression (D), IL-1β expression (D), and TNF-α expression (E).

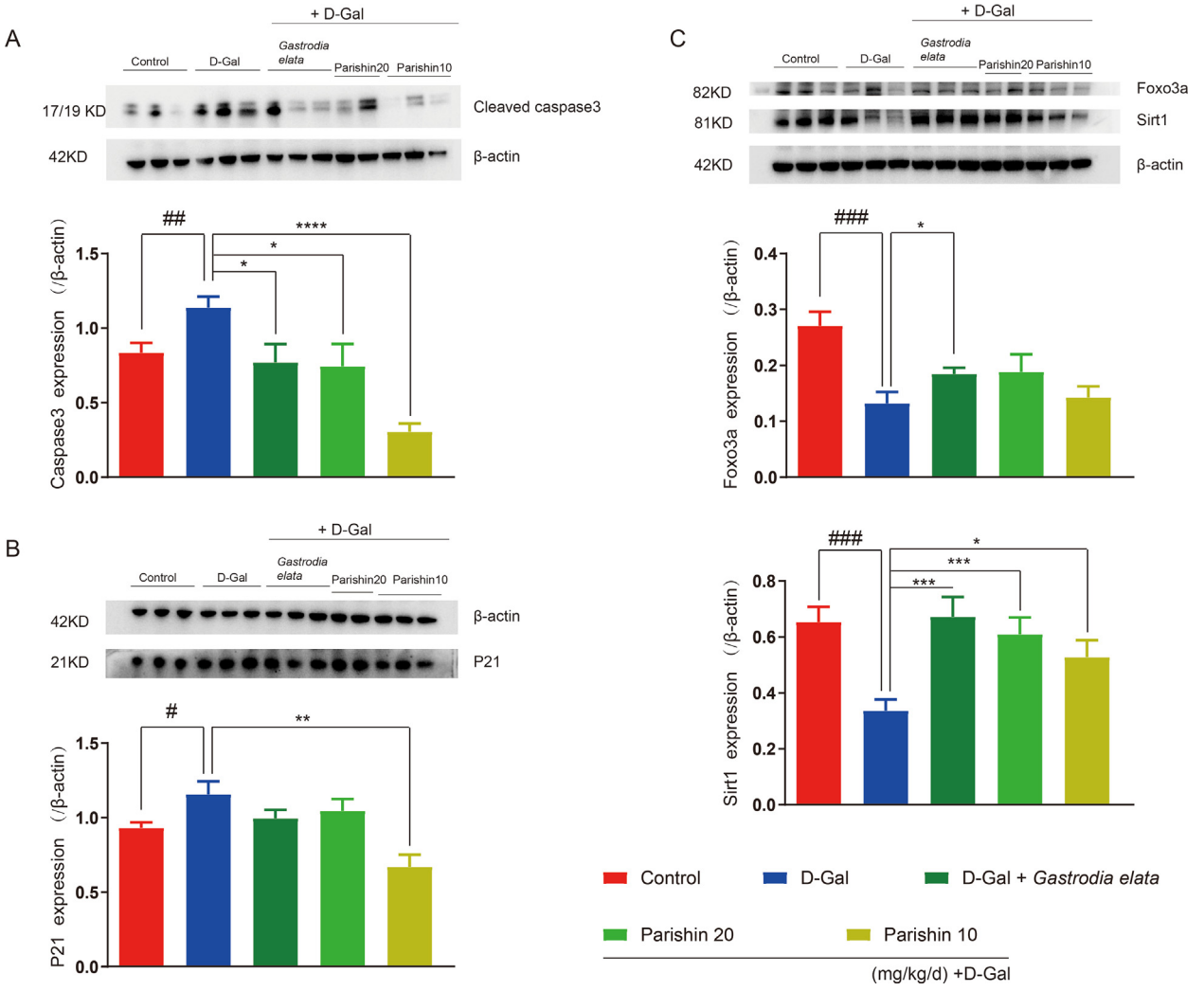

Fig. 10 Effect of *G. elata* and parishin on the protein expression level of aging-related biomarkers in the intestine analyzed by western blotting. (A) Effect of *G. elata* and parishin on the expression of CLEAVED CASPASE3. The histogram is the quantitative results of at least three repeats. ##, $p < 0.01$, represents significant differences between the control and D-Gal group. ****, $p < 0.0001$, *, $p < 0.05$, indicate significant differences between treatment groups and D-Gal group. (B) Effect of *G. elata* and parishin on the protein expression of P21. The histogram is the quantitative results of at least three repeats. #, $p < 0.05$, represents significant differences between the control group and D-Gal group. **, $p < 0.01$, indicates significant differences between treatment groups and D-Gal group. The not labeled groups were not significantly different compared to the D-Gal group. (C) Effect of *G. elata* and parishin on the expression of FOXO3A and SIRT1. The histogram is the quantitative results of at least three repeats. ###, $p < 0.001$, represents significant differences between the control and D-Gal groups. ***, $p < 0.001$, *, $p < 0.05$, indicate significant differences between treatment groups and D-Gal group. The not labeled groups were not significantly different compared to the D-Gal group.

best effect. Furthermore, the effects of *G. elata* and parishin were not strictly equivalent. This may be owing to the multi-component characteristic of *G. elata* and the non-equivalent dose. The dose of *G. elata* used was based on the dose used in clinical treatments for human dizziness and headache. According to the isolation of parishin, the dose of *G. elata* used here was roughly equivalent to 2.5 mg of parishin. This may explain why the effect of *G. elata* was not as good as that of 10 mg/kg/d parishin. However, these differences could also be attributed to the source of *G. elata*. It is well known that the origin, growing environment, and batch are all important factors to the effectiveness of traditional Chinese medicine. Therefore, the *G. elata* used for treatment and the isolated parishin may have different properties.

Analysis of the fecal microbiota composition showed that changes in the D-Gal group were mainly in three phyla, *Actinobacteria*, *Firmicutes*, and *Bacteroidetes* [Fig. S2]. Changes in *Firmicutes* and *Bacteroidetes* were similar to previously reported trends in aging-induced microbiota composition [13–15], and *G. elata* and parishin treatment could reverse these changes to different extents. In addition, the microbiota is simply structured in the infant period and dominated by *Bifidobacteria*, Enterobacteriaceae, and *Bacteroides*. Subsequently, more

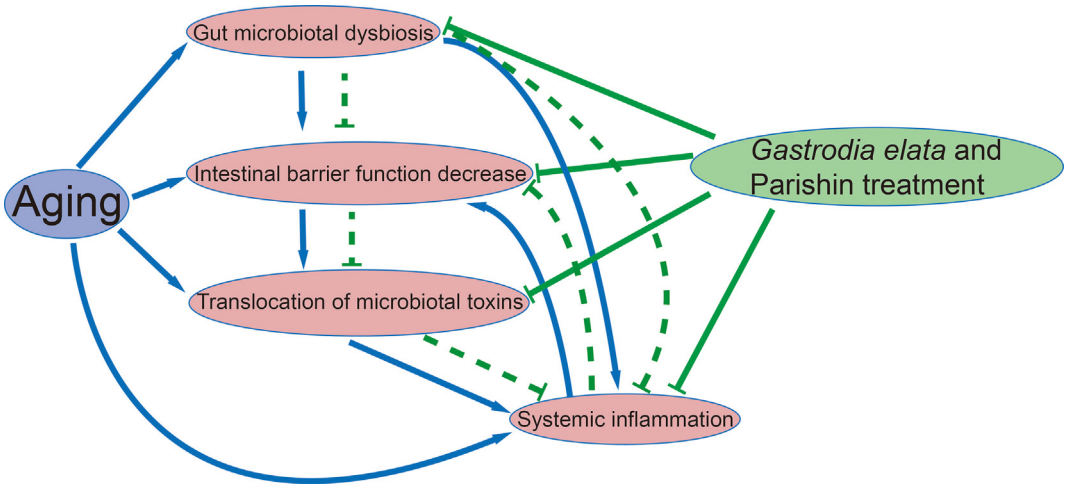

Fig. 11 Diagram of supposed mechanism of *G. elata* and parishin against gut aging.

species become part of the microbiota, increasing their diversity. After weaning, *Clostridiales* and *Bacteroidetes* dominate the microbiota [29]. A recent publication by Kim et al. has shown that *Clostridia* is the essential class of bacteria that provides colonization resistance; it protects mice against colonization with pathogens [30]. Our results showed that the *Clostridia* class and *Clostridiales* order had a downward trend in the D-Gal group compared with the control group, and *G. elata* and parishin treatments significantly reversed these changes [Fig. S2]. These results suggested that the administration of *G. elata* and parishin regulated the imbalance of the fecal microbiota. Furthermore, the results showed that for other significant changes in the fecal microbiota, including the *Erysipelotrichi* class and its included *Erysipelotrichales* and *Turicibacterales* orders, Erysipelotrichaceae and *Turicibacteraceae* families, *Allobaculum* and *Turicibacter* genus, *G. elata* and parishin effectively rescued the imbalance of these microbiotas. *Turicibacterales* and Erysipelotrichaceae are inflammation-related [31,32], indicating that *G. elata* and parishin could regulate the gut microbiota shift to a healthier state.

Aging induces gut microbiota dysbiosis, decreasing the intestinal barrier function and inflammatory state of the host. Gut microbiota dysbiosis can also decrease intestinal barrier function [16,17,19–21]. The decreased barrier function causes increased intestinal permeability, leading to intestinal endotoxin produced by gut microbiota translocation into the circulatory system, which aggravates the inflammatory state of the host [3]. In addition, gut microbiota dysbiosis may directly influence the expression of inflammatory cytokines [31,32]. Sustained inflammation can lead to dysregulation in the expression of TJP, resulting in barrier function defection and the entry of microbes [33,34] [Fig. 11]. In our study, the dysbiosis of LPS-producing microbiota, such as *Bacteroidetes*, and fatty acid-producing microbiota, such as *Firmicutes* and *Clostridia*, in D-Gal mice was recovered after *G. elata* and parishin administration. In addition, the abundances of inflammatory-related microbiota, *Turicibacterales* and Erysipelotrichaceae, and their corresponding orders and families were reversed by *G. elata* and parishin administration (Figs. 3 and S2]. Furthermore, *G. elata* and parishin prevented the decrease in intestinal barrier function and inflammatory cytokine expression [Figs. 1 and 5]. Based on these results, we propose that *G. elata* and parishin could ameliorate the inflammatory state and prevent the decreased barrier function by regulating the composition of the gut microbiota. The ameliorated inflammatory state may be helpful for the barrier function of the gut conversely. The protective effect on barrier function also inhibited the translocation of bacterial toxins and expression of systemic inflammatory cytokines [Fig. 11]. The gut microbiota composition, barrier function of the gut, and inflammatory state correlated with each other to maintain the health of the body. *G. elata* and parishin prevent gut aging through their feedforward relationships. Although we have not researched evidence to confirm this, the correlation analyses supported our proposition. Systemic inflammatory cytokines and *tjp2* expression was significantly correlated with *Turicibacterales*, *Erysipelotrichi and so on*, the abundance of which was significantly changed in aging mice and recovered after *G. elata* and parishin administration. Inflammatory cytokines expression was also correlated with *tjp2* expression. As the first barrier of the host, the protective effect on "leaky gut" also indicated that *G. elata* and parishin may protect other tissues against aging.

Conclusions

In summary, we showed that *G. elata* and parishin could ameliorate the decreased intestinal barrier function induced by D-Gal, and increase the abundance of SCFA-producing gut microbiota, including *Firmicutes* and *Clostridia*, while decreasing the abundance of LPS-producing and inflammatory-related gut microbiota, including *Bacteroidetes*, Erysipelotrichaceae, and *Turicibacterales*. The regulation of gut microbiota would further improve the barrier function and relieve the inflammatory state of the host. Based on the mutual correlations between barrier function, gut microbiota composition, and inflammation, we supposed that the mechanism of *G. elata* and parishin on gut aging was

attributed to the feedforward relationships among them. Furthermore, *G. elata* and parishin could reverse the expression of aging-related biomarkers, such as CLEAVED CASPASE3 and SIRT1. The results in this study strongly support the anti-aging effect of *G. elata* and parishin, which may be new candidates for anti-aging drug development. Further research should include exploring a novel strategy for quality evaluation, extraction optimization, and further application of *G. elata* to other related research aspects.

Compliance with ethics guidelines

This study was conducted according to the international ethical standards with guidance and approval from the Committee of the First Affiliated Hospital, College of Medicine, Zhejiang University (Permit Number: 20191094).

Funding

This work was supported by grants from the key discipline of Traditional Chinese Medicine in Zhejiang province [grant number 2017-XK-A31], the Zhejiang province science and technology plan of traditional Chinese medicine [grant number 2020ZQ031], and the National Nature Science Foundation of China [grant number 32000707].

Conflicts of interest

We declare no conflicts of interest.

Acknowledgments

We thank the core facilities of Zhejiang University Institute of Neuroscience, Protein Facility, Biochemical platform and Histomorphology platform of Zhejiang University School of Medicine for their technical support. We would like to thank Editage (www.editage.cn) for English language editing.

Appendix A. Supplementary data

Supplementary data to this article can be found online at https://doi.org/10.1016/j.bj.2022.07.001.

REFERENCES

[1] Campisi J, Kapahi P, Lithgow GJ, Melov S, Newman JC, Verdin E. From discoveries in ageing research to therapeutics for healthy ageing. Nature 2019;571:183–92.
[2] Nagpal R, Mainali R, Ahmadi S, Wang S, Singh R, Kavanagh K, et al. Gut microbiome and aging: physiological and mechanistic insights. Nutr Healthy Aging 2018;4:267–85.
[3] Fasano A. All disease begins in the (leaky) gut: role of zonulin-mediated gut permeability in the pathogenesis of some chronic inflammatory diseases. F1000Res 2020;9:69.
[4] Gong J, Hu M, Huang Z, Fang K, Wang D, Chen Q, et al. Berberine attenuates intestinal mucosal barrier dysfunction in type 2 diabetic rats. Front Pharmacol 2017;8:42.
[5] Mulak A, Bonaz B. Brain-gut-microbiota axis in Parkinson's disease. World J Gastroenterol 2015;21:10609–20.
[6] Licastro F, Candore G, Lio D, Porcellini E, Colonna-Romano G, Franceschi C, et al. Innate immunity and inflammation in ageing: a key for understanding age-related diseases. Immun Ageing 2005;2:8.
[7] Hooper LV, Littman DR, Macpherson AJ. Interactions between the microbiota and the immune system. Science 2012;336:1268–73.
[8] Ershler WB. Biological interactions of aging and anemia: a focus on cytokines. J Am Geriatr Soc 2003;51:S18–21.
[9] Madsen KL, Malfair D, Gray D, Doyle JS, Jewell LD, Fedorak RN. Interleukin-10 gene-deficient mice develop a primary intestinal permeability defect in response to enteric microflora. Inflamm Bowel Dis 1999;5:262–70.
[10] Adams RB, Planchon SM, Roche JK. IFN-gamma modulation of epithelial barrier function. Time course, reversibility, and site of cytokine binding. J Immunol 1993;150:2356–63.
[11] Al-Sadi R, Guo S, Ye D, Ma TY. TNF-alpha modulation of intestinal epithelial tight junction barrier is regulated by ERK1/2 activation of Elk-1. Am J Pathol 2013;183:1871–84.
[12] Ma TY, Iwamoto GK, Hoa NT, Akotia V, Pedram A, Boivin MA, et al. TNF-alpha-induced increase in intestinal epithelial tight junction permeability requires NF-kappa B activation. Am J Physiol Gastrointest Liver Physiol 2004;286:G367–76.
[13] Kumar M, Babaei P, Ji B, Nielsen J. Human gut microbiota and healthy aging: recent developments and future prospective. Nutr Healthy Aging 2016;4:3–16.
[14] Schiffrin EJ, Morley JE, Donnet-Hughes A, Guigoz Y. The inflammatory status of the elderly: the intestinal contribution. Mutat Res 2010;690:50–6.
[15] Biagi E, Nylund L, Candela M, Ostan R, Bucci L, Pini E, et al. Through ageing, and beyond: gut microbiota and inflammatory status in seniors and centenarians. PLoS One 2010;5:e10667.
[16] Thevaranjan N, Puchta A, Schulz C, Naidoo A, Szamosi JC, Verschoor CP, et al. Age-associated microbial dysbiosis promotes intestinal permeability, systemic inflammation, and macrophage dysfunction. Cell Host Microbe 2017;21:455–466 e4.
[17] Kim KA, Jeong JJ, Yoo SY, Kim DH. Gut microbiota lipopolysaccharide accelerates inflamm-aging in mice. BMC Microbiol 2016;16:9.
[18] Louis P, Flint HJ. Diversity, metabolism and microbial ecology of butyrate-producing bacteria from the human large intestine. FEMS Microbiol Lett 2009;294:1–8.
[19] Cani PD, Delzenne NM. The role of the gut microbiota in energy metabolism and metabolic disease. Curr Pharm Des 2009;15:1546–58.
[20] Yu LC, Wang JT, Wei SC, Ni YH. Host-microbial interactions and regulation of intestinal epithelial barrier function: from physiology to pathology. World J Gastrointest Pathophysiol 2012;3:27–43.
[21] Gao J, Xu K, Liu H, Liu G, Bai M, Peng C, et al. Impact of the gut microbiota on intestinal immunity mediated by tryptophan metabolism. Front Cell Infect Microbiol 2018;8:13.
[22] Park YM, Lee BG, Park SH, Oh HG, Kang YG, Kim OJ, et al. Prolonged oral administration of *Gastrodia elata* extract improves spatial learning and memory of scopolamine-treated rats. Lab Anim Res 2015;31:69–77.

[23] Xian JW, Choi AY, Lau CB, Leung WN, Ng CF, Chan CW. Gastrodia and Uncaria (tianma gouteng) water extract exerts antioxidative and antiapoptotic effects against cerebral ischemia in vitro and in vivo. Chin Med 2016;11:27.
[24] Hu Y, Li C, Shen W. Gastrodin alleviates memory deficits and reduces neuropathology in a mouse model of Alzheimer's disease. Neuropathology 2014;34:370–7.
[25] Lin Y, Sun Y, Weng Y, Matsuura A, Xiang L, Qi J. Parishin from gastrodia elata extends the lifespan of yeast via regulation of Sir2/Uth1/TOR signaling pathway. Oxid Med Cell Longev 2016;2016:4074690.
[26] Hsieh HM, Wu WM, Hu ML. Soy isoflavones attenuate oxidative stress and improve parameters related to aging and Alzheimer's disease in C57BL/6J mice treated with D-galactose. Food Chem Toxicol 2009;47:625–32.
[27] Guarente L. Calorie restriction and sirtuins revisited. Genes Dev 2013;27:2072–85.
[28] Morris BJ, Willcox DC, Donlon TA, Willcox BJ. FOXO3: a major gene for human longevity – a mini-review. Gerontology 2015;61:515–25.
[29] Backhed F, Roswall J, Peng Y, Feng Q, Jia H, Kovatcheva-Datchary P, et al. Dynamics and stabilization of the human gut microbiome during the first year of life. Cell Host Microbe 2015;17:690–703.
[30] Kim YG, Sakamoto K, Seo SU, Pickard JM, Gillilland MG 3rd, Pudlo NA, et al. Neonatal acquisition of Clostridia species protects against colonization by bacterial pathogens. Science 2017;356:315–9.
[31] Sun MF, Zhu YL, Zhou ZL, Jia XB, Xu YD, Yang Q, et al. Neuroprotective effects of fecal microbiota transplantation on MPTP-induced Parkinson's disease mice: gut microbiota, glial reaction and TLR4/TNF-alpha signaling pathway. Brain Behav Immun 2018;70:48–60.
[32] Kaakoush NO. Insights into the role of Erysipelotrichaceae in the human host. Front Cell Infect Microbiol 2015;5:84.
[33] Odenwald MA, Turner JR. The intestinal epithelial barrier: a therapeutic target? Nat Rev Gastroenterol Hepatol 2017;14:9–21.
[34] Marchiando AM, Graham WV, Turner JR. Epithelial barriers in homeostasis and disease. Annu Rev Pathol 2010;5:119–44.